

## Interfacial hydrodynamic instabilities driven by cross-diffusion in reverse microemulsions

M. A. Budroni, J. Carballido-Landeira, A. Intiso, A. De Wit, and F. Rossi

Citation: *Chaos* **25**, 064502 (2015); doi: 10.1063/1.4922186

View online: <http://dx.doi.org/10.1063/1.4922186>

View Table of Contents: <http://scitation.aip.org/content/aip/journal/chaos/25/6?ver=pdfcov>

Published by the [AIP Publishing](#)

---

### Articles you may be interested in

[Creating localized-droplet train by traveling thermal waves](#)

*Phys. Fluids* **26**, 082108 (2014); 10.1063/1.4892657

[Experimental study of a buoyancy-driven instability of a miscible horizontal displacement in a Hele-Shaw cell](#)

*Phys. Fluids* **26**, 044102 (2014); 10.1063/1.4870651

[Modeling the purging of dense fluid from a street canyon driven by an interfacial mixing flow and skimming flow](#)

*Phys. Fluids* **25**, 076603 (2013); 10.1063/1.4813786

[Spatio-temporal linear stability of double-diffusive two-fluid channel flow](#)

*Phys. Fluids* **24**, 054103 (2012); 10.1063/1.4718775

[Role of wall deformability on interfacial instabilities in gravity-driven two-layer flow with a free surface](#)

*Phys. Fluids* **22**, 094103 (2010); 10.1063/1.3480633

---



# Interfacial hydrodynamic instabilities driven by cross-diffusion in reverse microemulsions

M. A. Budroni,<sup>1,a)</sup> J. Carballido-Landeira,<sup>2,a)</sup> A. Intiso,<sup>3</sup> A. De Wit,<sup>2,b)</sup> and F. Rossi<sup>3,c)</sup>

<sup>1</sup>Department of Chemistry and Pharmacy, University of Sassari, Via Vienna 2, 07100 Sassari, Italy

<sup>2</sup>Nonlinear Physical Chemistry Unit, Service de Chimie Physique et Biologie Théorique, Université libre de Bruxelles, CP 231 - Campus Plaine, 1050 Brussels, Belgium

<sup>3</sup>Department of Chemistry and Biology, University of Salerno, via Giovanni Paolo II 132, 84084 Fisciano (SA), Italy

(Received 28 March 2015; accepted 25 May 2015; published online 9 June 2015)

When two microemulsions are put in contact in the gravity field along a horizontal contact line, cross-diffusion can trigger the transport of one species in the presence of a gradient in concentration of another species. We show here theoretically that such cross-diffusion effects can induce buoyancy-driven convective instabilities at the interface between two solutions of different compositions even when initially the less dense solution lies on top of the denser one. Two different sources of convective modes are identified depending whether positive or negative cross-diffusion is involved. We evidence the two predicted cross-diffusion driven instabilities experimentally using a two-layer stratification of Aerosol-OT (AOT) water-in-oil microemulsions solutions with different water or AOT composition. [<http://dx.doi.org/10.1063/1.4922186>]

**Aerosol-OT (AOT) microemulsions (MEs) have been well studied in the context of reaction-diffusion patterns in particular when the reactants of the oscillatory Belousov-Zhabotinsky (BZ) reaction are dissolved in it. Recently, such microemulsions have also proved to be good model systems to study, in the absence of any reaction, convective instabilities driven in the gravity field by cross-diffusion effects when gradients in a salt concentration triggers co-flow of water and AOT. Here, we show that even in a simpler three components water-AOT-octane system, cross-diffusion can trigger buoyancy-driven motions when a gradient of either water or AOT is imposed to an initially statically stable stratification of two different microemulsions. This paves the way to future understanding of cross-diffusion driven hydrodynamic instabilities and to studies of more complex reaction-diffusion-convection (RDC) patterns where convective effects could be induced by gradients in concentration inherent to reaction-diffusion patterns.**

## I. INTRODUCTION

New dynamical properties arising from the interplay of dissipative physico-chemical systems with dispersed media and soft matter are being studied since many years. The dynamics of the well known BZ<sup>1,2</sup> chemical oscillator, in particular, has been studied with many self-assembled matrices<sup>3</sup> and structured media<sup>4</sup> including gels and hydrogels,<sup>5–8</sup> micelles,<sup>9–14</sup> polymers,<sup>15–18</sup> and lipid vesicles and aggregates.<sup>19–24</sup>

<sup>a)</sup>M. A. Budroni and J. Carballido-Landeira contributed equally to this work.

<sup>b)</sup>Electronic mail: adewit@ulb.ac.be

<sup>c)</sup>Electronic mail: frossi@unisa.it

Particularly important from the pattern formation viewpoint, the AOT water-in-oil reverse MEs, are probably the most thoroughly studied system in combination with the BZ reaction. Microemulsions can be defined as optically clear, thermodynamically stable and isotropic liquid mixtures of an organic component (more commonly termed *oil*), water and surfactant (see the sketch in Figure 1(a) for the structure). In particular, in a reverse ME, the hydrophilic BZ reagents can be solubilized in water AOT-coated nano-droplets to create a great amount of coupled nano-oscillators. Early works dealt with the temporal behavior of the BZ reaction when

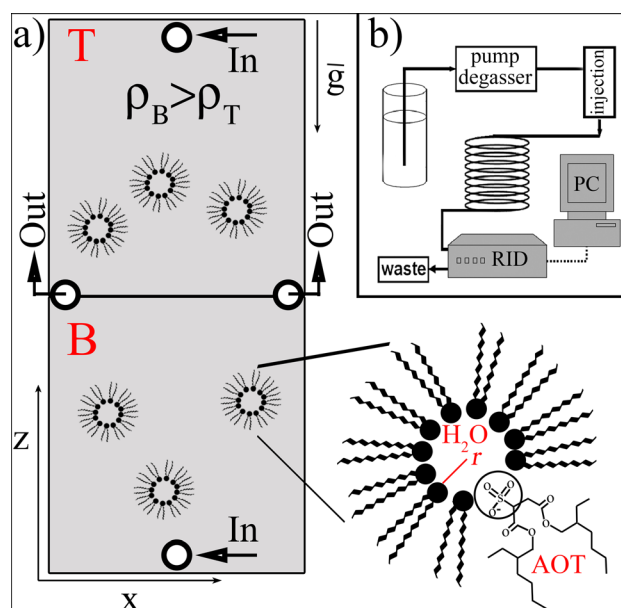


FIG. 1. (a) Sketch of the experimental configuration used for the Hele-Shaw experiments. (b) Scheme of the HPLC apparatus adapted for the Taylor dispersion measurements.

dissolved in the ME.<sup>25,26</sup> When the Brandeis group evidenced for the first time Turing structures and other exotic patterns in ME loaded with reactants of the BZ system in a spatially extended reactor,<sup>27–30</sup> the system attracted much more interest. The Brandeis group found that transport phenomena played a key role in the generation of the large amount of patterns observed in ME. Specifically, microemulsions induce two different diffusion modes for the BZ intermediates: slow diffusion for the hydrophilic activator, which can only move together with the droplets, and fast diffusion of the hydrophobic inhibitor, free to move alone into the oil phase with a diffusion coefficient two orders of magnitude larger than that of the activator. In order to generalize the modelling of the related pattern formation, cross-diffusion terms, i.e., the phenomenon by which a flux of a given species entrains the diffusive transport of another species,<sup>31</sup> were introduced in reaction-diffusion equations. In their seminal paper,<sup>32</sup> Vanag and Epstein introduce cross-diffusion phenomena in reaction-diffusion models, an aspect generally neglected in chemo-physical systems. In this context, the Brandeis group developed a new method to exploit the Taylor dispersion technique (TDT, see Sec. IB), in order to measure the diffusion matrix up to a 5-component microemulsion systems ( $\text{H}_2\text{O} + \text{AOT} + 2 \text{ BZ}$  reagents in octane as the oil phase)<sup>33–35</sup> and study the effect of cross-diffusion on the onset of Turing instabilities.<sup>35</sup>

Besides these breakthroughs in reaction-diffusion (RD) systems, I.R. Epstein has also pioneered the studies of RDC patterns in autocatalytic systems when convection develops around traveling fronts in solutions because of density gradients due to the exothermicity of the reaction and/or volume changes between reactants and products.<sup>36–39</sup>

With the idea that RD patterns and convective effects should be able to interact in microemulsions to give rise to a wealth of possible new RDC patterns and instabilities, we recently<sup>40</sup> started investigating hydrodynamic convective patterns triggered by cross-diffusion in microemulsions in the absence of any reaction. The objective is twofold: first, the ME system is a perfect model system to explore new convective modes related to the introduction of cross-diffusion effects in the analysis of hydrodynamic instabilities of miscible two-layer systems. Even though some early works have started addressing this problem in polymers,<sup>41,42</sup> cross-diffusion driven convective instabilities in the absence of any reaction are still poorly understood. The second objective is to understand which convective modes can be observed in microemulsions before starting to add the complexity of RD patterning to construct new RDC patterns. In this context, we first studied<sup>40</sup> fingered convective motions developing at the interface between two identical AOT-ME in a gravitational field, when the lower denser solution contains a simple water-soluble molecule ( $\text{NaBrO}_3$ ) free to diffuse towards the upper less dense layer and generate by cross diffusion a positive co-flux of both water and AOT. In detail, when  $\text{NaBrO}_3$  diffused from the bottom to the upper layer, it dragged along both  $\text{H}_2\text{O}$  and AOT molecules thus generating a non-monotonic density distribution around the contact line, destabilizing convectively an initially stable system. By means of a diffusion model, we explained the dependence of

the hydrodynamic patterns upon  $[\text{NaBrO}_3]$  cross-diffusion and we opened a new path to study the coupling between pattern formation due to RD and RDC interactions in microemulsions systems.

In this paper, we show that cross-diffusion drives convective instabilities in an initial statically stable stratification between two microemulsions (without any added salt) in a Hele-Shaw cell by just imposing a gradient in water or AOT concentration. By using the TDT, we characterise the diffusion matrix of the Water/AOT mixture and show how ME represent a convenient model to study cross-diffusion-driven convection. On the basis of Fick's equations including cross-diffusion coefficients, we predict two different possible convective instability scenarios based on the sign of the cross-diffusion terms. We use these results to devise experiments where the species free to diffuse from one layer to the other present either positive or negative cross-diffusion coefficients. We demonstrate experimentally the difference in convective patterns for the two predicted instability scenarios and compare the properties of the obtained convective patterns.

The paper is structured as follows, in Sec. IA, we briefly sketch transport properties of a microemulsion system. In Sec. IB, the main features of the Taylor dispersion method are described. The experimental methods and setup are presented in Sec. II while results are discussed in Sec. III. In particular, in Sec. III A, the diffusion matrices of the Water/AOT systems investigated are characterised. In Secs. III B 1 and III B 2, we introduce a theoretical approach to cross-diffusion-driven convection and, by analyzing the shape of the density profiles, we characterize two classes of instability scenarios that are next demonstrated experimentally in Sec. III C. Finally, conclusions are drawn in Sec. IV.

## A. Transport processes in microemulsions

Sodium bis(2-ethylhexyl) sulfosuccinate, usually referred to as Aerosol-OT, or simply AOT, is able to feature stable reverse microemulsions in a simple three-component system for a broad range of compositions. The geometry of the dispersed domains may range from spherical or elongated droplets to lamellar phases, through interconnected channels of various length and local topology. The exact shape of the water and oil pseudophases depends upon a number of factors, such as chemical nature and concentration of the microemulsion components, temperature and pressure. However, at fixed temperature and pressure, the structural properties of AOT reverse microemulsions can be basically described by two parameters:<sup>27</sup>

- the water to AOT molar concentration ratio  $\omega = [\text{H}_2\text{O}]/[\text{AOT}]$  which, in the case of droplets, gives an estimation of the water core radius,  $R_w$ , expressed in nanometers, according to the relation<sup>30</sup>  $R_w \simeq 0.17\omega$ .
- the volume fraction of the dispersed phase  $\phi_d = \phi_{\text{H}_2\text{O}} + \phi_{\text{AOT}}$  which can be used as an indicator of the interactions among water domains. In fact, higher values of  $\phi_d$  result in clusters formation and eventually in the onset of a continuous aqueous phase (percolation threshold<sup>30,43</sup>  $\phi_d \sim 0.5 - 0.6$ ).

In a ternary system like ME (H<sub>2</sub>O (Species 1)/AOT (Species 2) + Octane as the solvent), the diffusion matrix consists of 4 elements: 2 diagonal main diffusion coefficients ( $D_{11}$  and  $D_{22}$ ), which account for the motion of water and AOT in octane, respectively, according to their own concentration gradient and 2 off diagonal cross-diffusion coefficients ( $D_{12}$  and  $D_{21}$ ), related to the motion of water generated by a gradient of AOT and *vice versa*. Diffusion is therefore described by a set of two equations and four diffusion coefficients as

$$J_1 = -D_{11}\nabla C_1 - D_{12}\nabla C_2, \quad (1)$$

$$J_2 = -D_{21}\nabla C_1 - D_{22}\nabla C_2, \quad (2)$$

where  $J_i$  is the flux of the  $i$  species and  $C_1$  and  $C_2$  are the concentrations of H<sub>2</sub>O and AOT, respectively.

The cross-diffusion coefficients were found to be necessary to describe in detail ME systems, in particular, a flux of AOT generates a large co-flux of water ( $D_{12}$  positive), while the flux of H<sub>2</sub>O generates a counter-flux of AOT ( $D_{21}$  negative).<sup>44–46</sup> The presence of solutes in ME also generates large cross-diffusion effects, which were measured up to a 5 components system.<sup>33–35</sup> Excluded volume effects are the most important mechanisms in generating cross diffusion in ME, because the motion of AOT or H<sub>2</sub>O changes the size of the droplets' water core influencing the actual concentration of the two species. Further mechanisms related with the size of the water droplets are, however, at play.<sup>34,45</sup>

## B. The Taylor dispersion technique

The TDT<sup>47–50</sup> is a fast and reliable method for measuring the diffusion coefficients of solutes in one- or multi-component solutions.<sup>33–35,45,51,52</sup> The TDT is based on the diffusive spreading of a drop of solution injected into a laminarly flowing stream of the same mixture but with slightly different concentrations. A small volume of the perturbing solution is injected into the flowing eluent at the entrance of a long capillary tube having a radius  $R_0$ . As it moves along the tube at a constant speed  $u_0$  (cm/s), the injected sample is deformed by the flow and by radial diffusion. If the flow has a parabolic velocity profile, the drop spreads out into a shape that can be fitted by a combination of  $n$  Gaussian functions for an  $(n + 1)$ -component system ( $n$  solutes + 1 solvent). The eluted peak is monitored by a suitable detector, chosen according to the composition of the analyzed samples. The diffusion coefficients are calculated from the parameters of the Gaussian functions that fit the eluted peak.

Taylor demonstrated that if the elution process is slow enough, the radial variation of the sample concentration is small relative to the axial variation and the concentration profile of the  $i$ -th species ( $c_i$ ) in a  $n$ -component system can be described with a one-dimensional equation ( $c_i$  is averaged over the cross section of the tube) taking the form<sup>33,47</sup>

$$\frac{\partial c_i}{\partial t} = \sum_{j=1}^n F_{ij} \frac{\partial^2 c_j}{\partial z^2}, \quad (3)$$

where  $F_{ij}$  are called dispersion coefficients. They have the same units as the molecular diffusion coefficients  $D_{ij}$  (cm<sup>2</sup> s<sup>-1</sup>) and are related to them through the relation

$$F_{ij} = \frac{R_0^2 u_0^2}{48 \det(\mathbf{D})} \det(\mathbf{M}_{D_{ji}}) (-1)^{(i+j)}, \quad (4)$$

$\det(\mathbf{D})$  is the determinant of the  $n \times n$  diffusion matrix  $\mathbf{D}$  and  $\det(\mathbf{M}_{D_{ji}})$  is the determinant of the minor associated with element  $D_{ji}$  of  $\mathbf{D}$ .

The  $F_{ij}$  can be obtained from the experimentally found parameters characterizing the Gaussian fit to eluted peaks:  $P_{i,exp}$ ,  $K_i$ , and  $\sigma_i$  through the following equation:

$$l_0^{-1} \sum_{i=1}^n \sigma_i P_{i,exp} = \sum_{j=1}^n c_{j0} \sum_{i=1}^n K_i F_{ij}, \quad (5)$$

where  $l_0$  (cm) is the length of the capillary occupied by the sample injected at the initial time ( $l_0^{-1} = \pi R_0^2 / V_0$ ,  $V_0$  is the injected volume),  $P_{i,exp}$  are the pre-exponential parts of the Gaussian,  $\sigma_i$  are the dispersions of the Gaussian functions which are equal to the eigenvalues of the dispersion matrix  $\mathbf{F}$ ,  $c_{j0}$  is the difference between the concentration of component  $j$  in the injected sample and in the carrier stream,  $K_i$  is the instrumental sensitivity with respect to that component (typically linear in the concentration). The experimentally measurable quantities  $P_{i,exp}$ ,  $K_i$ , and  $\sigma_i$  can be found by fitting all the experimental peak curves  $v(t)$  (generated with injections of different compositions) according to

$$v(t) = \sum_{i=1}^n \frac{P_{i,exp}}{\sqrt{4\pi\sigma_i t}} \exp\left[-\frac{u_0^2(t-t_0)^2}{4\sigma_i t}\right], \quad (6)$$

where  $u_0$  is the mean velocity of the carrier stream and  $t_0$  is the retention time. The coefficients  $K_i$  can be found by analyzing different experiments involving injections with only one  $c_{i0} \neq 0$  as

$$K_i = l_0^{-1} \left( \sum_{j=1}^n P_{j,exp} \right) / c_{i0} \quad i = 1 \dots n. \quad (7)$$

## II. EXPERIMENTAL SETUPS

### A. Taylor dispersion setup

In all experiments, a 15 m silica glass dispersion capillary (inner radius  $R_0 = (0.016 \pm 0.002)$  cm) was placed between the injector and the cell of the differential flow-through thermostated refractive index detector, RID (Agilent G1362A). The RID measures the difference between the refractive index of the eluent which is present in a reference cell and the refractive index of the flowing solution containing the sample, which passes through a measuring cell. The refractive index is, in fact, dependent on the composition of the system and, for dilute solutions, it is a linear combination of the refractive index of each component weighted by its concentration.

In order to eliminate small bubbles from the solutions, an inline ion exchange resin based de-gasser (Agilent G1322A) was placed between the eluent reservoir and the pump.

The tubing was coiled in a 30 cm diameter helix and immersed in a thermostated water-bath (Julabo ME-16G), kept at 25 °C. The eluent flow was kept steady and constant at 0.015 mL/min by using an isocratic pump (Agilent G1310B). A 2  $\mu$ L sample loop was used for samples injection. The detector was connected to a personal computer for data acquisition.

Solutions were prepared by using bidistilled water, AOT (Aldrich) was of analytical grade and used as received. Octane (Sigma) was further purified by mixing with concentrated sulfuric acid for seven days.

Samples were injected every 60 min to avoid the overlapping of the peaks. Experimental peaks generated with different injections were simultaneously fitted, by using the Levenberg-Marquardt algorithm,<sup>53</sup> to equation (6). In order to correct the instrumental drift, a baseline of the form ( $a + bt$ ) was previously subtracted from the recorded signals with the help of a suitable software.

## B. Hele-Shaw cell

The experimental reactor used to study convective dynamics at the interface between two MEs of different compositions consists of a vertically oriented Hele-Shaw cell, composed of two borosilicate glasses separated by a spacer of 0.10 mm (Figure 1(a)).<sup>54</sup> Two different water-in-oil (W/O) reverse microemulsions were filled in the reactor through the inlet ports positioned at the top and the bottom of the cell (“In” arrows in Fig. 1(a)). The excess of the solutions is pumped out through the cell’s outlets (“Out” arrows in Fig. 1(a)) until a flat interface between the two liquids is obtained. Each of the two microemulsions having different composition initially occupies half of the reactor height. The top and bottom solutions are prepared at room temperature ( $\sim 21$  °C) by means of distilled water and of a 1.5 M AOT in octane stock solution, conveniently diluted until the desired  $\phi_d$  (0.16–0.20) is reached. The top and bottom microemulsions are prepared at slightly different droplet sizes ( $\omega = 8$ –14), with the bottom solution always denser than the top one. Different  $\omega$  ratios are obtained by varying the amount of H<sub>2</sub>O (AOT) while keeping the amount of AOT (H<sub>2</sub>O) constant.

The dynamics of the interface is tracked by using the Schlieren technique,<sup>40,55</sup> which allows to observe the gradients in the refractive index between both microemulsions, due to their density differences and, therefore, monitor the convective motions in solutions without the presence of dyes.

The solutal expansion coefficient of each  $i$ -component ( $i = \text{H}_2\text{O}$ , AOT) was determined according to  $\alpha_i = \frac{1}{\rho_0} \frac{\partial \rho}{\partial C_i}$ , where  $\rho_0$  is the density of the solvent (octane) and  $C_i$  the molar concentration of the  $i$ -th species. In order to measure these coefficients, the volume of both the solvent and of one of the components was fixed, while the concentration of the other was gradually increased. The densities were measured

by using an Anton Paar densimeter and it was found that the solutal expansion coefficients were 0.0051 M<sup>-1</sup> for H<sub>2</sub>O and 0.154 M<sup>-1</sup> for AOT.

## III. RESULTS

### A. Diffusion matrices

In order to characterize the diffusion matrix of the microemulsions used for the Hele-Shaw experiments, three systems below the percolation limit were investigated; namely, microemulsions with the smallest and the largest value for the concentration ratio,  $\omega$ , and the volume fraction,  $\phi_d$ , (8.15; 0.165) and (14; 0.2), respectively, and one composition in the middle of the interval, (11.84; 0.18). Several experiments were performed by injecting samples with an excess of one (H<sub>2</sub>O or AOT) or two components. All Taylor dispersion peaks obtained were then simultaneously fitted using Eq. (6) with  $i = 1, 2$  to extract the experimental parameters ( $P_{i,exp}$ ,  $\sigma_i$ ). As an example, Figure 2 shows the peaks obtained by injecting samples with an excess of only AOT ( $\blacktriangle$ ) or only H<sub>2</sub>O ( $\blacksquare$ ) into a carrier stream of microemulsion with  $\omega = 14$  and  $\phi_d = 0.2$ . The sensitivity coefficients  $K_i$  were found by introducing the fitted parameters in Eq. (7). By using Eq. (5), we find the dispersion coefficients  $F_{ij}$  and finally, by using Eq. (4) we transform  $F_{ij}$  to diffusion coefficients  $D_{ij}$ . The complete procedure to fine-tune the diffusion matrix values is reported elsewhere.<sup>33</sup>

Table I reports the diffusion matrices of the investigated systems, which span the whole range of the microemulsions composition used for the Hele-Shaw cell experiments. Since both  $\omega$  and  $\phi_d$  have been varied simultaneously, it is difficult to find a clear trend for the dependence of  $D_{ij}$  upon the system composition. However, for the purpose of this work, we were more interested in finding the nature and the order of

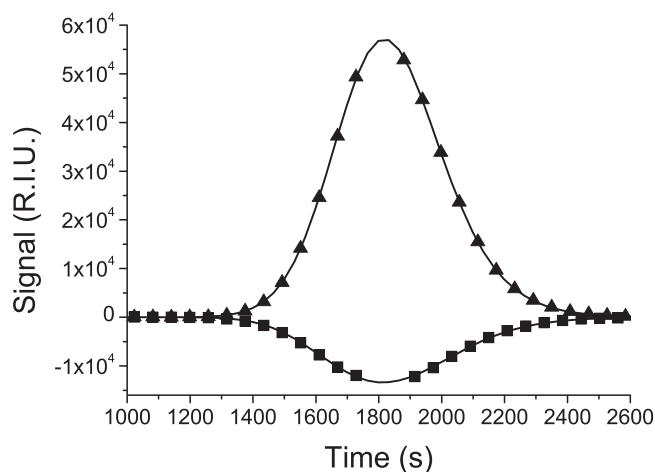


FIG. 2. Taylor dispersion peaks for the system H<sub>2</sub>O/AOT/octane. ( $\blacktriangle$ ) Experimental peak for a sample containing an excess of AOT,  $\Delta[\text{AOT}] = 0.1$  M,  $\Delta[\text{H}_2\text{O}] = 0$  M. ( $\blacksquare$ ) Experimental peak for a sample containing an excess of H<sub>2</sub>O,  $\Delta[\text{AOT}] = 0$  M,  $\Delta[\text{H}_2\text{O}] = 2$  M. The composition of the eluent is  $[\text{H}_2\text{O}] = 4.38$  M,  $[\text{AOT}] = 0.31$  M and  $[\text{octane}] = 5.14$  M ( $\omega = 14$  and  $\phi_d = 0.2$ ),  $T = 25$  °C. Solid lines are the best fit obtained with sum of two Gaussian curves with  $P_{1,exp} = 1.4 \times 10^7$  R.I.U.  $\times$  cm,  $P_{2,exp} = 1.7 \times 10^7$  R.I.U.  $\times$  cm ( $\blacktriangle$ ) and  $P_{1,exp} = -2 \times 10^5$  R.I.U.  $\times$  cm,  $P_{2,exp} = -7 \times 10^6$  R.I.U.  $\times$  cm ( $\blacksquare$ ). For both peaks,  $\sigma_1 = 6$  cm<sup>2</sup>/s,  $\sigma_2 = 12$  cm<sup>2</sup>/s,  $K_1 = -2.85 \times 10^6$  R.I.U./M and  $K_2 = 1.07 \times 10^8$  R.I.U./M.

TABLE I. Ternary diffusion coefficients (in  $10^{-6}$  cm<sup>2</sup>/s) for the H<sub>2</sub>O ( $i = 1$ )/AOT ( $i = 2$ )/Octane systems at different  $\omega$  and  $\phi_d$ .

$\omega$	$\phi_d$	$D_{11}$	$D_{12}$	$D_{21}$	$D_{22}$
8.15	0.165	$0.8 \pm 0.1$	$3.6 \pm 1.0$	$-0.0015 \pm 0.0020$	$1.10 \pm 0.01$
11.84	0.18	$0.60 \pm 0.04$	$7.8 \pm 2.0$	$-0.010 \pm 0.002$	$1.30 \pm 0.04$
14	0.2	$0.3 \pm 0.1$	$1.1 \pm 0.2$	$-0.005 \pm 0.004$	$0.96 \pm 0.01$

magnitude of the cross-diffusion coefficients to be used in simulations (see Sec. III B). The results reported in Table I fit well with literature data determined for other compositions of the microemulsions,<sup>33–35,44,45</sup> in particular, we find that the motion of AOT generates large co-fluxes of water ( $D_{12}$  large and positive) and the motion of water generates small counter-fluxes of AOT ( $D_{21}$  small and negative) for all the parameters range explored in the Hele-Shaw experiments.

## B. Theoretical approach

### 1. Cross-diffusion model

The possible convective instabilities which take place around the horizontal interface between two microemulsions in a vertical Hele-Shaw cell (Figure 1(a)) can be interpreted by studying the corresponding temporal evolution of one-dimensional density profiles along the vertical axis  $Z$ , where the gravitational acceleration  $\bar{g}$  is oriented downwards. The density profiles give qualitative information about the instabilities to be expected, as their morphology shows whether and where local regions of denser fluid overlying less dense zones may develop along the gravitational axis.

Consider a spatial domain of length  $L_Z$  where a solution  $T$  of density  $\rho^T$ , containing the solute 1 (H<sub>2</sub>O) with the initial concentration  $C_{1,0}^T$  and the solute 2 (AOT) with concentration  $C_{2,0}^T$  is placed on top of the solution  $B$ , with concentration  $C_{1,0}^B = C_{1,0}^T$ ,  $C_{2,0}^B > C_{2,0}^T$  (or *vice versa*, depending on the type of cross-diffusion we are interested in). The density  $\rho^B$  is always larger than  $\rho^T$  in order to start from a stable configuration with regard to a Rayleigh-Taylor instability.<sup>56</sup> Upon contact, the two miscible solutions, initially separated along the horizontal interface  $z = L_Z/2$ , start mixing by diffusion. The diffusion of each species is affected by concentration gradients in the other one and hence the spatio-temporal dynamics of the system obeys a set of fickian equations including the cross-diffusive terms of the diffusion matrix  $\mathbf{D}$

$$\partial_t C_1 = D_{11} \nabla^2 C_1 + D_{12} \nabla^2 C_2, \quad (8)$$

$$\partial_t C_2 = D_{21} \nabla^2 C_1 + D_{22} \nabla^2 C_2. \quad (9)$$

Although main ( $D_{ii}$ ) and cross-diffusion coefficients ( $D_{ij}$ ,  $i \neq j$ ) depend on the chemical composition of the system (Table I), as a first approximation, we consider them here as constant.<sup>35,40</sup>

We solve Eqs. (8) and (9) with a constant concentration of either water or AOT and a jump in the concentration of the other specie centered around  $z = L_Z/2$  as initial condition. No-flux boundary conditions are imposed at the borders of the spatial domain. We obtain numerically the concentration profiles  $C_1(z, t)$  and  $C_2(z, t)$  which are next used to

reconstruct the related density profiles according to the state equation

$$\rho(C_1, C_2) = \rho^T (1 + \alpha_1 (C_1 - C_{1,0}^T) + \alpha_2 (C_2 - C_{2,0}^T)). \quad (10)$$

This expansion relies on the assumption that concentrations slightly change with respect to the initial composition of the reference top solution with density  $\rho^T$  and we can then admit a linear dependence of the global density  $\rho$  upon the solute concentration. In Eq. (10),  $\alpha_i = \frac{1}{\rho^T} \frac{\partial \rho}{\partial C_i}$  is the solutal expansion coefficient of the  $i$ -th species.

### 2. Density profiles analysis

The double-layer initial condition represents a key specificity of the cross-diffusion problem under study. Depending upon the starting concentration profile of the two species, we can “select” a specific cross-diffusion path and, in turn, the related convective dynamics. For instance, when a concentration jump is initially imposed to AOT at constant water content, this induces a diffusive motion in the initially homogeneous distribution of H<sub>2</sub>O *via* the cross-diffusion term  $D_{12}$ , while the other cross-diffusion term ( $D_{21}$ ) plays a negligible influence. In particular, species 2 (AOT) generates a co-flux of the species 1 (water) since  $D_{12}$  is positive. *Vice versa*, when the initial concentration jump is imposed on water at constant AOT, cross-diffusion effects, triggered by the propagation of water towards the upper layer, influence the evolution of AOT as controlled by  $D_{21} < 0$ . In this case, the diffusion of H<sub>2</sub>O generates a counter-flux of AOT.

These mechanisms are shown in Fig. 3. Both panels (a) and (b) describe in the first two graphs the spatio-temporal evolution of the species concentration starting from one of the two initial configurations under analysis; the third graph displays the resulting density profiles. The concentration profiles are obtained by solving in one spatial dimension ( $z$ ) the diffusion equations with the characteristic diffusion matrix of the ME (see Sec. III A)

$$\mathbf{D} = \begin{pmatrix} 0.6 & 7.8 \\ -0.01 & 1.3 \end{pmatrix} \times 10^{-6} \text{cm}^2 \text{s}^{-1}, \quad (11)$$

while the density distribution is found according to Eq. (10), using the solutal expansion coefficients measured experimentally (see Sec. II):  $\alpha_{\text{H}_2\text{O}} = 0.0051 \text{M}^{-1}$  and  $\alpha_{\text{AOT}} = 0.154 \text{M}^{-1}$ . Fig. 3(a) illustrates how the diffusion of species 1, featuring an initial concentration jump, generates a counter-flux of species 2 ruled by the negative cross-diffusivity  $D_{21} = -0.01 \times 10^{-6} \text{cm}^2 \text{s}^{-1}$ . In the concentration profile  $C_2(z, t)$ , this induces a local depletion area in the upper layer and a symmetric accumulation of species 2 just below the initial interface  $L_Z/2$ . By contrast, when the initial concentration jump is imposed to the AOT (species 2) (Fig. 3(b)), its diffusion from the bottom to the upper layer promotes a co-flux of the water (species 1), quantified by the positive cross-diffusivity  $D_{12} = 7.8 \times 10^{-6} \text{cm}^2 \text{s}^{-1}$ . As a result, the concentration profile  $C_1(z, t)$  develops a non-monotonic shape with a local maximum and a minimum symmetrically located above and below the initial interface,

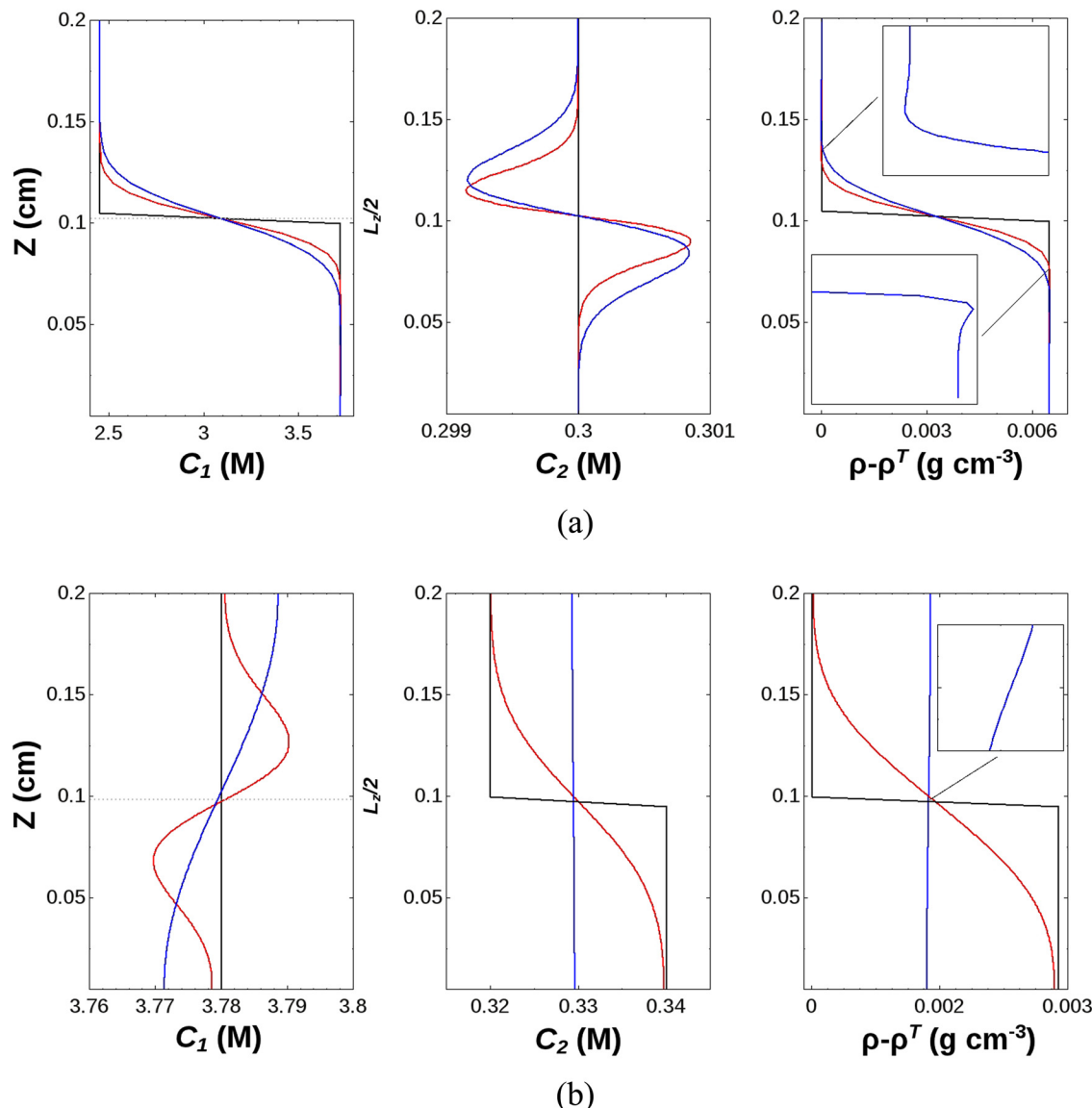


FIG. 3. Spatio-temporal evolution of the concentration profiles  $C_1(z, t)$ ,  $C_2(z, t)$  and of the density excess  $(\rho - \rho^T(z))$ . In each graph, we show with black lines the initial distribution of the variables, while red and blue profiles depict the spatial concentration and density at intermediate and long times, respectively. (a) NCC mechanism due to the negative cross-diffusion term ( $D_{21}$ ) and induced by means of a concentration jump in the species 1 (water). (b) PCC scenario with positive cross-diffusion ( $D_{12}$ ) triggered by the upwards diffusion of the species 2 (AOT).

respectively. We clearly observe an inversion in the morphology of the non-monotonic density profiles depending whether the initial jump is imposed on species 1 (water) or species 2 (AOT), as this activates different cross-diffusion terms with opposite sign.

Non-monotonic density profiles will develop because of cross-diffusion effects provided a sufficient influence of the non-monotonic concentration to the global density. In the first case (Fig. 3(a)), though the small negative cross-diffusion  $D_{21}$  drives the formation of concentration extrema of small amplitude in  $C_2(z, t)$ , the AOT has a large weight ( $\alpha_{AOT}$ ) to the density and we can identify a minimum and a maximum above and below the interface, respectively. This profile is reminiscent of typical density profiles characterizing Diffusive Layer Convection (DLC) scenarios<sup>56,57</sup> and we can expect that, starting from an initial constant AOT concentration and a jump in  $H_2O$ , convective modes will grow

in the upper and the lower layer, without deforming the initial contact line between the two stratified solutions. We will refer to this scenario as Negative Cross-diffusion-driven Convection (NCC).

Analogous considerations can be drawn for the opposite initial configuration shown in Fig. 3(b). Here, the cross-diffusion term responsible for the non-monotonic evolution of  $C_1(z, t)$ ,  $D_{12}$ , is positive and large. This means that  $C_1(z, t)$  can develop concentration extrema but, since  $H_2O$  presents a small relative contribution to the system density, the smoothing of the initial AOT gradient must be waited to observe the influence of  $H_2O$  in the density evolution. Fig. 3(b) (third panel) allows to appreciate how, starting from an initial condition in which the density increases downwards the gravitational axis, the density profile changes in time into a monotonically decreasing profile. In real experiments, this results in a fingered deformation of the initial interface and

hereunder we refer to this scenario as Positive Cross-diffusion-driven Convection (PCC).

### C. Hele-Shaw results

In order to confirm the theoretical predictions, we performed experiments in a Hele-Shaw cell by stratifying two microemulsions with different initial concentrations of water and AOT. In all experiments, we start from an initial statically stable stratification, i.e., the microemulsion located in the bottom is denser than the one on the top. We explore two different scenarios to analyze the negative (NCC) and positive (PCC) cross-diffusive-driven instabilities. In the negative cross-diffusive case (Fig. 3(a)), the AOT concentration is initially constant everywhere while the microemulsion on the top has less water than that placed below, as depicted in Figure 4(a). When the difference in water concentration is relatively small ( $\Delta[H_2O]_{\text{bottom-top}} < 0.75$  M), we do not observe any buoyant instability. This can be understood as a limitation of our experimental device in discerning small gradients in the refractive index. However, for larger gradients ( $0.75 \text{ M} < \Delta[H_2O]_{\text{bottom-top}} < 1.75$  M), the initially stable configuration becomes unstable after 5–6 minutes exhibiting convective vortices at symmetric distances above and below the unperturbed interface (Figures 4(b)–4(d), features that compare favorably with the classification given in Sec. III B for the same initial configuration (NCC scenario). We recover the typical nonlinear dynamics of DLC modes where convective vortices develop at symmetric distances above and below the unperturbed interface.<sup>56,57</sup> We track the evolution of the mixing zone, defined as the distance between the most upwards and downwards tip of the fingers. Figure 5 demonstrates that the larger the initial jump in water concentration the slower the mixing of the microemulsions. This is expected as the cross-diffusion effects have then to overcome a larger stabilizing density jump to promote convection.

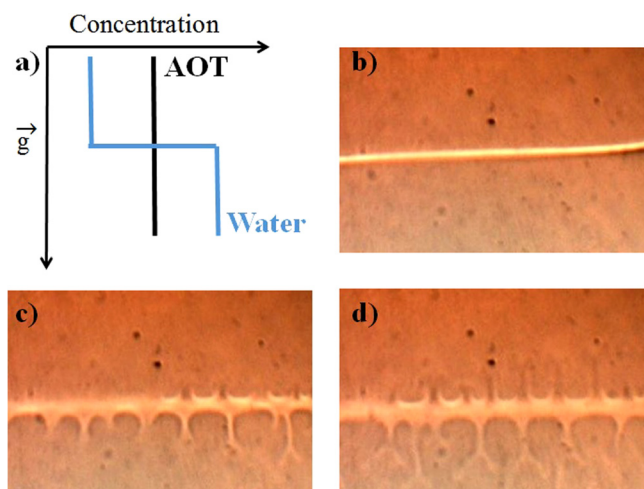


FIG. 4. Experimental negative cross-diffusive instability. (a) Sketch of the experimental initial conditions required to achieve negative cross-diffusion. (b)–(d) Three snapshots showing the evolution of the DLC mode obtained with  $\Delta[H_2O]_{\text{bottom-top}} = 1.15$  M taken at  $t = 0, 700$  and  $1200$  s.  $ME_T \omega = 8.15, \phi_d = 0.165$ ;  $ME_B \omega = 12.2, \phi_d = 0.185$ . Frame sizes (b)–(d) =  $11.45 \text{ mm} \times 8.9 \text{ mm}$ .

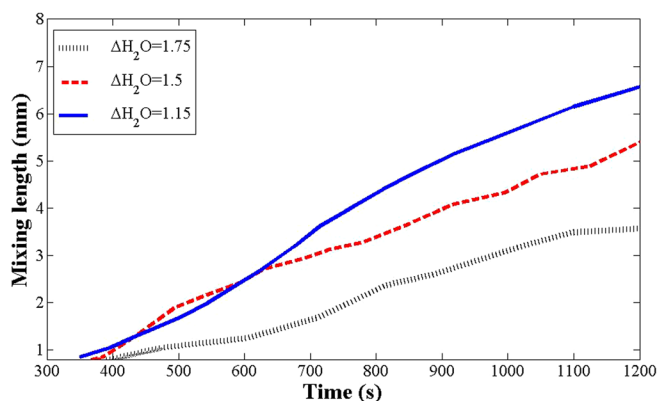


FIG. 5. Temporal evolution of mixing length for different values of the initial water concentration jump.

In order to analyze the positive cross-diffusive (PCC) driven convective instability, we start with a jump on the AOT surfactant concentration between both microemulsions at a homogeneous amount of water, as sketched in Figure 6(a). By imposing a surfactant jump in the range  $0.02 \text{ M} < \Delta AOT_{\text{bottom-top}} < 0.06 \text{ M}$ , the initial contact line deforms into equally separated fingers that grow vertically with time at the interface (Figures 6(b)–6(d)). These structures are successfully predicted by the analysis of the density profile obtained from the cross-diffusion model in analogous conditions (PCC scenario) and can be better perceived by performing spatio-temporal plots along the horizontal and vertical axis (Figure 7). Horizontally, along the initial contact line between both microemulsions (dashed line in Figure 7(a)), we observe how convective fingers (vertically oriented white stripes in Figure 7(c)) have a characteristic hydrodynamic wavelength. This feature, defined as the average distance between consecutive convective fingers, has been calculated before being altered due to the appearance of lateral flows in the system. Analysis at different density jumps between both microemulsions show that the larger the initial

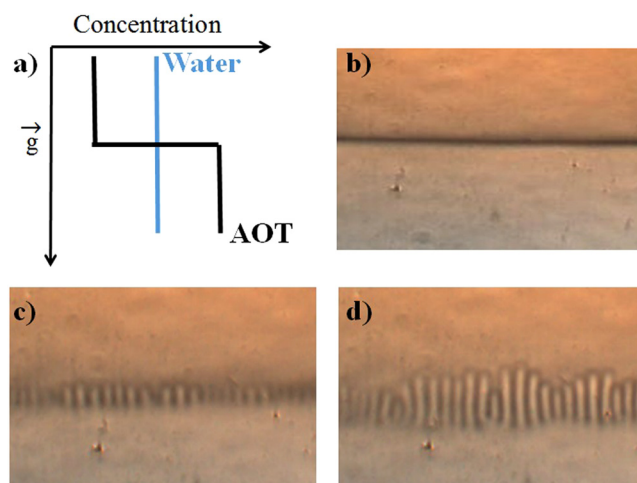


FIG. 6. Experimental positive cross-diffusive instability. (a) Sketch of the experimental initial concentration of a jump of AOT between both microemulsions while the water concentration is constant. (b)–(d) Three snapshots taken at  $t = 0, 700$ , and  $1250$  s displaying the evolution of double diffusive modes obtained with  $\Delta AOT_{\text{bottom-top}} = 0.06$  M.  $ME_T \omega = 11.95, \phi_d = 0.19$ ;  $ME_B \omega = 9.8, \phi_d = 0.2$ . Frame sizes (b)–(d) =  $11.45 \text{ mm} \times 8.9 \text{ mm}$ .

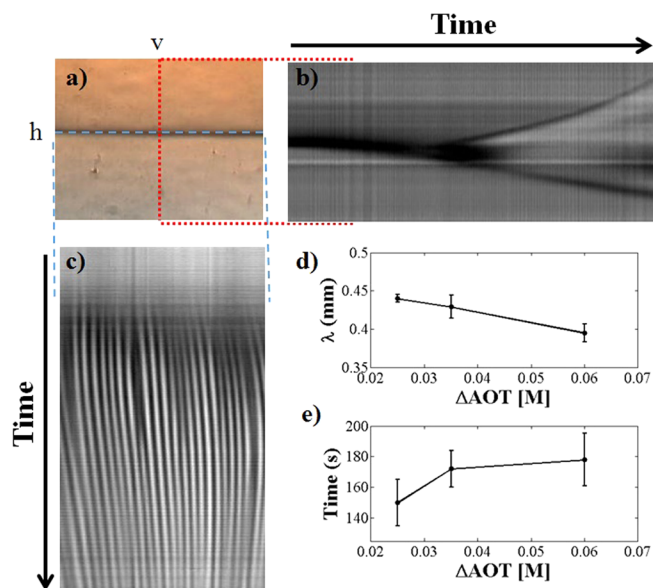


FIG. 7. Analysis of positive cross-diffusive driven instability. (a) Initial frame (1.45 mm  $\times$  8.9 mm) displaying the horizontal contact line between two microemulsions carried out at  $\phi_d = 0.18$  and  $\Delta AOT_{\text{bottom-top}} = 0.06$  M. (b) Spatio-temporal dynamics obtained along the vertical red dotted line  $v$  showing the deformation of the contact line along the gravitational axis. Frame size = 8.9 mm  $\times$  2000 s. (c) Spatio-temporal plot constructed along the horizontal line  $h$  demonstrating the emergence of fingers at different locations of the interface and their temporal evolution. Frame size = 11.45 mm  $\times$  2000 s. Variation of wavelength (d) and induction time (e) for different initial jumps in the AOT concentration between the bottom and top microemulsions. A solid line was drawn in (d) and (e) to help the reader following the data trend.

jump in AOT concentration the smaller the wavelength as reported in Figure 7(d). The vertical space-time plot (Figure 7(b)) accounts for the induction period, defined as the interval of time that convective fingers require to develop. This characteristic time is shortened as the initial jump in AOT concentration is reduced (Figure 7(e)). Furthermore, Figure 7(b) gives us information about the asymmetric growth rate of convective fingers (90  $\mu\text{m}/\text{min}$  for ascending fingers in contrast to 75  $\mu\text{m}/\text{min}$  for the descending ones).

#### IV. CONCLUDING DISCUSSION

To conclude, through a combined experimental and theoretical study, we have demonstrated that ME are a simple and ideal model system where different convective instabilities driven by 2-component cross-diffusion can be induced. Thanks to the TDT method, we have first characterized the AOT-H<sub>2</sub>O diffusion matrix of the microemulsion solutions for the concentrations used in the HS cell convective experiments. These measurements show that the diffusion matrix consists of a positive  $D_{12}$  and a negative  $D_{21}$  cross-diffusion term and that there is a suitable concentration range where H<sub>2</sub>O and AOT can be varied without changing dramatically the actual values of the diffusion coefficients. With this information and knowing the solutal expansion coefficients of the two species, we could theoretically predict two possible cross-diffusion driven convective scenarios, depending upon which species features the initial concentration jump in the

starting statically stable stratification. When the initial concentration jump is imposed on the water concentration, DLC-type convective patterns grow driven by the negative cross-diffusivity  $D_{21}$  (NCC). On the contrary, DD-type of instabilities can develop in time in the presence of an initial concentration jump introduced in AOT when the cross-diffusion dynamics is controlled by the positive  $D_{12}$  (PCC).

The positive and negative cross-diffusion-driven convective scenarios have been described on the basis of one-dimensional density profiles directly constructed using experimental data. By studying the spatial dependence of these density profiles, we can also interpret some features obtained from the analysis of experimental data. For instance, in our simulations, we find that the time needed to form the monotonically decreasing profile in the PCC (featuring a denser fluid over a less dense medium, like the blue profile in Fig. 3(b) (third panel)) is independent of the initial concentration jump imposed to the AOT. By contrast, the related density jump,  $\Delta\rho$ , which measures the maximal density difference between the top and the bottom layer as  $\max\left(\left\{\frac{\rho(L_z,t)-\rho(0,t)}{\rho(0,t)}\right\}\forall t\right)$ , slightly increases with  $\Delta[AOT]$  (Fig. 8). Considering the experimental error, these features are substantially recovered in the characterization of the experiments shown in Figs. 7(d) and 7(e). Here, we cannot recognise any significant trend in the onset time of the instability (the average value is almost constant) while, the decreasing drifting of the pattern wavelength with  $\Delta[AOT]$  can be ascribed to the increasing magnitude of  $\Delta\rho$ . The larger this initial density jump, the more intense the resulting convective dynamics and, in turn, the shorter the characteristic wavelengths to be expected.

Our results can be generalised to any multi-component system showing either positive or negative cross-diffusion terms in the diffusion matrix  $\mathbf{D}$ . Similar results have been found for polymer-sugar systems<sup>41</sup> and polymer-polyelectrolytes systems,<sup>58</sup> both showing positive cross-diffusion terms due to an excluded volume mechanism. Microemulsions allowed us to investigate, for the first time, the effect of negative cross-diffusion on the development of hydrodynamic instabilities and we found that the sign of the cross-diffusion coefficients is important to select the type of

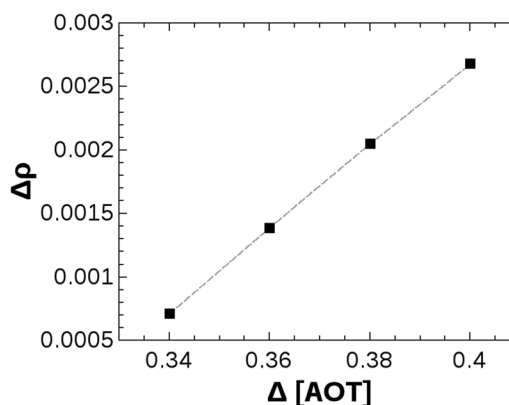


FIG. 8. Dependence upon  $\Delta[AOT]$  of the maximal density jump ( $\Delta\rho$ ) between the top and the bottom layer in the monotonically decreasing profile developing in the PCC scenario.

instability. These results also show that microemulsions will be a suitable experimental model to investigate the coupling among reaction-driven and diffusion-driven hydrodynamic instabilities.

## ACKNOWLEDGMENTS

J.C.-L. acknowledges financial support from FRS-FNRS. A.D. acknowledges support from Prodex and from FRS-FNRS for the FORECAST project. F.R. acknowledges support from the University of Salerno (projects ORSA133584 and ORSA149477). M.A.B. gratefully acknowledges Regione Sardegna for financial support in the framework of “Asse IV Capitale Umano, Obiettivo Operativo 1.3 Linea di Attività 1.3.1 del P.O.R. Sardegna F.S.E. 2007/2013—Progetti in forma associata e/o partenariale C.U.P. E85E12000060009.”

- <sup>1</sup>B. P. Belousov, “A periodic reaction and its mechanism,” in *Sbornik Referatov po Radiatsionno Meditsine* (Medgiz, Moscow, 1958), pp. 145–147.
- <sup>2</sup>A. M. Zhabotinsky, “Periodic liquid phase reactions,” *Proc. Acad. Sci. USSR* **157**, 392–395 (1964).
- <sup>3</sup>F. Rossi and M. L. Turco Liveri, “Chemical self-organization in self-assembling biomimetic systems,” *Ecol. Modell.* **220**, 1857–1864 (2009).
- <sup>4</sup>I. R. Epstein, V. K. Vanag, A. C. Balazs, O. Kuksenok, P. Dayal, and A. Bhattacharya, “Chemical oscillators in structured media,” *Acc. Chem. Res.* **45**, 2160–2168 (2011).
- <sup>5</sup>T. Yamaguchi, L. Kunhert, Z. Nagy-Ungvarai, S. C. Müller, and B. Hess, “Gel systems for the Belousov-Zhabotinskii reaction,” *J. Phys. Chem.* **95**, 5831–5837 (1991).
- <sup>6</sup>R. Yoshida, T. Takahashi, T. Yamaguchi, and H. Ichijo, “Self-oscillating gel,” *J. Am. Chem. Soc.* **118**, 5134–5135 (1996).
- <sup>7</sup>Y. Takeoka, M. Watanabe, and R. Yoshida, “Self-sustaining peristaltic motion on the surface of a porous gel,” *J. Am. Chem. Soc.* **125**, 13320–13321 (2003).
- <sup>8</sup>Y. Zhang, N. Li, J. Delgado, N. Zhou, R. Yoshida, S. Fraden, I. R. Epstein, and B. Xu, “Structural modulation of self-oscillating gels: changing the proximity of the catalyst to the polymer backbone to tailor chemo-mechanical oscillation,” *Soft Matter* **8**, 7056–7061 (2012).
- <sup>9</sup>A. Paul, “Observations of the effect of anionic, cationic, neutral, and zwitterionic surfactants on the Belousov-Zhabotinsky reaction,” *J. Phys. Chem. B* **109**, 9639–9644 (2005).
- <sup>10</sup>F. Rossi, R. Varsalona, and M. L. Turco Liveri, “New features in the dynamics of a ferroin-catalyzed Belousov-Zhabotinsky reaction induced by a zwitterionic surfactant,” *Chem. Phys. Lett.* **463**, 378–382 (2008).
- <sup>11</sup>F. Rossi, R. Lombardo, L. Sciascia, C. Sbriziolo, and M. L. Turco Liveri, “Spatio-temporal perturbation of the dynamics of the ferroin catalyzed Belousov-Zhabotinsky reaction in a batch reactor caused by sodium dodecyl sulfate micelles,” *J. Phys. Chem. B* **112**, 7244–7250 (2008).
- <sup>12</sup>R. A. Jahan, K. Suzuki, H. Mahara, S. Nishimura, T. Iwatsubo, A. Kaminaga, Y. Yamamoto, and T. Yamaguchi, “Perturbation mechanism and phase transition of AOT aggregates in the Fe(II)[batho(SO<sub>3</sub>)<sub>2</sub>]<sub>3</sub>-catalyzed aqueous Belousov-Zhabotinsky reaction,” *Chem. Phys. Lett.* **485**, 304–308 (2010).
- <sup>13</sup>F. Rossi, R. Varsalona, N. Marchettini, and M. L. Turco Liveri, “Control of spontaneous spiral formation in a zwitterionic micellar medium,” *Soft Matter* **7**, 9498 (2011).
- <sup>14</sup>F. Rossi, M. A. Budroni, N. Marchettini, and J. Carballido-Landeira, “Segmented waves in a reaction-diffusion-convection system,” *Chaos* **22**, 037109 (2012).
- <sup>15</sup>J. A. Pojman and Q. Tran-Cong-Miyata, *Nonlinear Dynamics in Polymeric Systems*, ACS Symposium Series Vol. 869 (ACS, Washington DC, 2004).
- <sup>16</sup>L. Sciascia, F. Rossi, C. Sbriziolo, M. L. Turco Liveri, and R. Varsalona, “Oscillatory dynamics of the Belousov-Zhabotinsky system in the presence of a self-assembling nonionic polymer. Role of the reactants concentration,” *Phys. Chem. Chem. Phys.* **12**, 11674–11682 (2010).
- <sup>17</sup>R. Tamate, T. Ueki, M. Shibayama, and R. Yoshida, “Self-oscillating vesicles: Spontaneous cyclic structural changes of synthetic diblock copolymers,” *Ang. Chem. Int. Ed.* **53**, 11248–11252 (2014).
- <sup>18</sup>T. P. de Souza and J. Perez-Mercader, “Entrapment in giant polymersomes of an inorganic oscillatory chemical reaction and resulting chemo-mechanical coupling,” *Chem. Commun.* **50**, 8970–8973 (2014).
- <sup>19</sup>S. Ristori, F. Rossi, G. Biosa, N. Marchettini, M. Rustici, and E. Tiezzi, “Interplay between the Belousov-Zhabotinsky reaction-diffusion system and biomimetic matrices,” *Chem. Phys. Lett.* **436**, 175–178 (2007).
- <sup>20</sup>G. Biosa, S. Ristori, O. Spalla, M. Rustici, and M. J. B. Hauser, “Macroscopic dynamics as reporter of mesoscopic organization: The Belousov-Zhabotinsky reaction in aqueous layers of dppe lamellar phases,” *J. Phys. Chem. A* **115**, 3227–3232 (2011).
- <sup>21</sup>S. Thutupalli, S. Herminghaus, and R. Seemann, “Bilayer membranes in micro-fluidics: from gel emulsions to soft functional devices,” *Soft Matter* **7**, 1312 (2011).
- <sup>22</sup>R. Tomasi, J.-M. Noel, A. Zenati, S. Ristori, F. Rossi, V. Cabuil, F. Kanoufi, and A. Abou-Hassan, “Chemical communication between liposomes encapsulating a chemical oscillatory reaction,” *Chem. Sci.* **5**, 1854–1859 (2014).
- <sup>23</sup>P. Stano, F. Wodlei, P. Carrara, S. Ristori, N. Marchettini, and F. Rossi, “Approaches to molecular communication between synthetic compartments based on encapsulated chemical oscillators,” in *Advances in Artificial Life and Evolutionary Computation*, Communications in Computer and Information Science No. 445, edited by C. Pizzuti and G. Spezzano (Springer International Publishing, 2014), pp. 58–74.
- <sup>24</sup>F. Rossi, A. Zenati, S. Ristori, J.-M. Noel, V. Cabuil, F. Kanoufi, and A. Abou-Hassan, “Activatory coupling among oscillating droplets produced in microfluidic based devices,” *Int. J. Unconvention. Comput.* **11**, 21–34 (2015).
- <sup>25</sup>D. Balasubramanian and G. Rodley, “Incorporation of chemical oscillators into organized surfactant assemblies,” *J. Phys. Chem.* **92**, 5995–5998 (1988).
- <sup>26</sup>V. K. Vanag and D. V. Boulanov, “Behavior of the Belousov-Zhabotinskii oscillator in reverse micelles of AOT in octane,” *J. Phys. Chem.* **98**, 1449–1453 (1994).
- <sup>27</sup>V. K. Vanag and I. R. Epstein, “Pattern formation in a tunable medium: The Belousov-Zhabotinsky reaction in an aerosol OT microemulsion,” *Phys. Rev. Lett.* **87**, 228301 (2001).
- <sup>28</sup>V. K. Vanag and I. R. Epstein, “Inwardly rotating spiral waves in a reaction-diffusion system,” *Science* **294**, 835–837 (2001).
- <sup>29</sup>V. K. Vanag and I. R. Epstein, “Segmented spiral waves in a reaction-diffusion system,” *Proc. Natl. Acad. Sci. U.S.A.* **100**, 14635–14638 (2003).
- <sup>30</sup>V. K. Vanag, “Waves and patterns in reaction-diffusion systems. Belousov-Zhabotinsky reaction in water-in-oil microemulsions,” *Phys. Usp.* **47**, 923–941 (2004).
- <sup>31</sup>E. L. Cussler, *Diffusion: Mass Transfer in Fluid Systems* (Cambridge University Press, Cambridge, New York, 2009).
- <sup>32</sup>V. K. Vanag and I. R. Epstein, “Cross-diffusion and pattern formation in reaction-diffusion systems,” *Phys. Chem. Chem. Phys.* **11**, 897–912 (2009).
- <sup>33</sup>V. K. Vanag, F. Rossi, A. Cherkashin, and I. R. Epstein, “Cross-diffusion in a water-in-oil microemulsion loaded with malonic acid or ferroin. Taylor dispersion method for four-component systems,” *J. Phys. Chem. B* **112**, 9058–9070 (2008).
- <sup>34</sup>F. Rossi, V. K. Vanag, E. Tiezzi, and I. R. Epstein, “Quaternary cross-diffusion in water-in-oil microemulsions loaded with a component of the Belousov-Zhabotinsky reaction,” *J. Phys. Chem. B* **114**, 8140–8146 (2010).
- <sup>35</sup>F. Rossi, V. K. Vanag, and I. R. Epstein, “Pentary cross-diffusion in water-in-oil microemulsions loaded with two components of the Belousov-Zhabotinsky reaction,” *Chem. A Eur. J.* **17**, 2138–2145 (2011).
- <sup>36</sup>J. A. Pojman and I. R. Epstein, “Convective effects on chemical waves. 1. Mechanisms and stability criteria,” *J. Phys. Chem.* **94**, 4966–4972 (1990).
- <sup>37</sup>J. A. Pojman, I. R. Epstein, T. J. McManus, and K. Showalter, “Convective effects on chemical waves. 2. Simple convection in the iodate-arsenous acid system,” *J. Phys. Chem.* **95**, 1299–1306 (1991).
- <sup>38</sup>J. A. Pojman, I. P. Nagy, and I. R. Epstein, “Convective effects on chemical waves. 3. Multicomponent convection in the iron(ii)-nitric acid system,” *J. Phys. Chem.* **95**, 1306–1311 (1991).

- <sup>39</sup>I. R. Epstein and J. A. Pojman, *An Introduction to Nonlinear Chemical Dynamics: Oscillations, Waves, Patterns, and Chaos* (Oxford University Press, New York, 1998).
- <sup>40</sup>M. A. Budroni, L. Lemaigre, A. De Wit, and F. Rossi, "Cross-diffusion-induced convective patterns in microemulsion systems," *Phys. Chem. Chem. Phys.* **17**, 1593–1600 (2015).
- <sup>41</sup>B. N. Preston, T. C. Laurent, W. D. Comper, and G. J. Checkley, "Rapid polymer transport in concentrated solutions through the formation of ordered structures," *Nature* **287**, 499–503 (1980).
- <sup>42</sup>S. Sasaki, "Development of coupled molecular diffusion to convective fingering," *J. Phys. Chem.* **100**, 20164–20171 (1996).
- <sup>43</sup>E. V. Alvarez, J. Carballido-Landeira, J. Guiu-Souto, P. Taboada, and A. P. Muñuzuri, "Modulation of volume fraction results in different kinetic effects in Belousov-Zhabotinsky reaction confined in AOT-reverse microemulsion," *J. Chem. Phys.* **134**, 094512 (2011).
- <sup>44</sup>D. Leaist and L. Hao, "Size distribution model for chemical interdiffusion in water AOT heptane water-in-oil microemulsions," *J. Phys. Chem.* **99**, 12896–12901 (1995).
- <sup>45</sup>D. G. Leaist, "Relating multicomponent mutual diffusion and intradiffusion for associating solutes. Application to coupled diffusion in water-in-oil microemulsions," *Phys. Chem. Chem. Phys.* **4**, 4732–4739 (2002).
- <sup>46</sup>L. Costantino, C. D. Volpe, O. Ortona, and V. Vitagliano, "Isothermal diffusion in a peculiar ternary system: The microemulsion AOT-water-heptane," *J. Chem. Soc., Faraday Trans.* **88**, 61–63 (1992).
- <sup>47</sup>G. Taylor, "Dispersion of soluble matter in solvent flowing slowly through a tube," *Proc. R. Soc. London, Ser. A* **219**, 186–203 (1953).
- <sup>48</sup>R. Aris, "On the dispersion of a solute in a fluid flowing through a tube," *Proc. R. Soc. London, Ser. A* **235**, 67–77 (1956).
- <sup>49</sup>A. Alizadeh, C. Nieto de Castro, and W. Wakeham, "The theory of the Taylor dispersion technique for liquid diffusivity measurements," *Int. J. Thermophys.* **1**, 243–284 (1980).
- <sup>50</sup>W. Price, "Theory of the Taylor dispersion technique for three-component-system diffusion measurements," *J. Chem. Soc., Faraday Trans. 1* **84**, 2431–2439 (1988).
- <sup>51</sup>R. Callendar and D. G. Leaist, "Diffusion coefficients for binary, ternary, and polydisperse solutions from peak-width analysis of Taylor dispersion profiles," *J. Solution Chem.* **35**, 353–379 (2006).
- <sup>52</sup>L. Chen and D. G. Leaist, "Multicomponent Taylor dispersion coefficients," *J. Solution Chem.* **43**, 2224–2237 (2014).
- <sup>53</sup>P. E. Gill and W. Murray, "Algorithms for the solution of the nonlinear least-squares problem," *SIAM J. Numer. Anal.* **15**, 977–992 (1978).
- <sup>54</sup>Y. Shi and K. Eckert, "A novel Hele-Shaw cell design for the analysis of hydrodynamic instabilities in liquid-liquid systems," *Chem. Eng. Sci.* **63**, 3560–3563 (2008).
- <sup>55</sup>G. S. Settles, *Schlieren and Shadowgraph Techniques* (Springer, Berlin, 2001).
- <sup>56</sup>P. M. J. Trevelyan, C. Almarcha, and A. De Wit, "Buoyancy-driven instabilities of miscible two-layer stratifications in porous media and Hele-Shaw cells," *J. Fluid Mech.* **670**, 38–65 (2011).
- <sup>57</sup>J. Carballido-Landeira, P. M. J. Trevelyan, C. Almarcha, and A. De Wit, "Mixed-mode instability of a miscible interface due to coupling between Rayleigh-Taylor and double-diffusive convective modes," *Phys. Fluids* **25**, 024107 (2013).
- <sup>58</sup>H. Maeda, K.-i. Nakamura, H. Yamane, S. Sasaki, and R. Kakehashi, "Counterion condensation and rapid transport of polyelectrolytes through aqueous polymer solutions," *Colloids Surf. A* **440**, 131–135 (2014).